Human Molecular Genetics, 2017, Vol. 26, No. 15 2933–2948

doi: 10.1093/hmg/ddx179
Advance Access Publication Date: 8 May 2017
Original Article

ORIGINAL ARTICLE

Vps35 in cooperation with LRRK2 regulates synaptic vesicle endocytosis through the endosomal pathway in *Drosophila*

Tsuyoshi Inoshita[1], Taku Arano[2], Yuka Hosaka[3], Hongrui Meng[4], Yujiro Umezaki[4], Sakiko Kosugi[5], Takako Morimoto[5], Masato Koike[6], Hui-Yun Chang[7], Yuzuru Imai[1,3,*] and Nobutaka Hattori[1,3,*]

[1]Department of Research for Parkinson's Disease, [2]Center for Genomic and Regenerative Medicine, Juntendo University Graduate School of Medicine, Tokyo 113-8421, Japan, [3]Department of Neurology, Juntendo University Graduate School of Medicine, Tokyo 113-8421, Japan, [4]Research Institute for Diseases of Old Age, Juntendo University Graduate School of Medicine, Tokyo 113-8421, Japan, [5]Laboratory of Cellular Neurobiology, Tokyo University of Pharmacy and Life Science, Hachioji, Tokyo 192-0392, Japan, [6]Department of Cell Biology and Neuroscience, Juntendo University Graduate School of Medicine, Tokyo 113-8421, Japan and [7]Institute of Systems Neuroscience and Department of Medical Science, National Tsing Hua University, Hsinchu 30013, Taiwan, Republic of China

*To whom correspondence should be addressed at: Department of Research for Parkinson's Disease, Juntendo University Graduate School of Medicine, 2-1-1 Hongo, Bunkyo-ku, Tokyo 113-8421, Japan. Tel: +81 368018332; Fax: +81 358000547; Email: yzimai@juntendo.ac.jp (Y.I.); Department of Neurology, Juntendo University Graduate School of Medicine, 2-1-1 Hongo, Bunkyo-ku, Tokyo 113-8421, Japan. Tel: +81 358022731; Fax: +81 358000547; Email: nhattori@juntendo.ac.jp (N.H.)

Abstract

Mutations of the retromer component Vps35 and endosomal kinase LRRK2 are linked to autosomal dominant forms of familial Parkinson's disease (PD). However, the physiological and pathological roles of Vps35 and LRRK2 in neuronal functions are poorly understood. Here, we demonstrated that the loss of *Drosophila* Vps35 (dVps35) affects synaptic vesicle recycling, dopaminergic synaptic release and sleep behavior associated with dopaminergic activity, which is rescued by the expression of wild-type dVps35 but not the PD-associated mutant dVps35 D647N. *Drosophila* LRRK2 dLRRK together with Rab5 and Rab11 is also implicated in synaptic vesicle recycling, and the manipulation of these activities improves the *Vps35* synaptic phenotypes. These findings indicate that defects of synaptic vesicle recycling in which two late-onset PD genes, *Vps35* and *LRRK2*, are involved could be key aspects of PD etiology.

Introduction

Vps35, a component of the retromer complex involved in Rab GTPase-mediated vesicular transport, is a gene product responsible for an autosomal dominant form of familial Parkinson's disease (PD) with middle or late onset (1,2). The complex of Vps35 with Vps29 and Vps26 is implicated in cargo sorting and membrane tubulation (3,4), and its function appears to be evolutionarily conserved from yeast to human (5). The amino acid residue where a missense mutation D620N was found in PD

Received: February 27, 2017. **Revised:** April 17, 2017. **Accepted:** May 4, 2017

worldwide is conserved among species, including *Drosophila*. Although the mutation Vps35 D620N itself is not affected in the formation of the complex with Vps29 and Vps26, it impairs the binding with the FAM21-containing WASH (Wiskott-Aldrich Syndrome Protein and SCAR Homolog) complex (6), which drives the F-actin-mediated tubule scission of endosomes (7,8).

LRRK2 is a kinase with multiple domains, including a leucine-rich repeat domain, a small GTPase domain, a COR domain and a WD40 domain. The missense mutations of LRRK2 are responsible for late-onset PD. LRRK2 is localized in endosomes (9), which suggests its roles in membrane dynamics (10–13). *Drosophila* has a copy of the orthologue of LRRK2 dLRRK, which is also localized at the endosomes (14). The loss of dLRRK causes the accumulation of enlarged early endosomes and abnormally expanded late endosomal and lysosomal structures (15), whereas LRRK2/dLRRK is involved in the Rab5-mediated early and Rab11-mediated recycling endosomal pathway, regulating the turnover of a Notch ligand Delta (16). The roles of LRRK2/dLRRK in neuronal synapses are also suggested, where it is implicated in the morphogenesis of synapses and endocytosis of synaptic vesicles (SVs) (17–22). The transgenic expression of dVps35 rescues PD-associated mutant forms of LRRK2-mediated dopaminergic neuronal loss in *Drosophila* (11,23), whereas the colocalization of LRRK2 and Vps35 was not observed in mammalian cultured cells in another study (24). Therefore, the molecular mechanism underlying a suppression effect of Vps35 in neurotoxicity caused by LRRK2 mutations remains unknown.

Here, we report that synaptic endocytosis is regulated by the close cooperation of LRRK2 and Vps35, in which Rab5 and Rab11 are involved. Our findings suggest that dysfunction of synaptic dynamics is an early event of neurodegeneration in PD.

Results

dVps35 and dLRRK cooperatively regulate synaptogenesis

We generated human Vps35 (hVps35) transgenic fly lines that carry wild-type (WT) and pathogenic D620N mutant forms of Vps35 with GAL4-responsible UAS sequences and dVps35 UAS-transgenic lines for WT and D647N (DN, corresponding to D620N in humans) (Fig. 1A). Because the homozygous null mutation of the *dVps35* gene leads to death in the prepupal stage (25), we examined whether hVps35 functionally rescues the lethality of *dVps35*-null flies. Despite its evolutionarily conserved property, ubiquitous expression of any forms of hVps35 using the *Da-GAL4* driver did not suppress the lethality, suggesting that hVps35 does not act functionally in *Drosophila*. In contrast, the ubiquitous expression of both dVps35 WT and DN rescued the lethality (Fig. 1B). Although it was suggested that both Vps35 WT and DN are incorporated in the retromer complex with the same efficiency (7,8), overexpressed dVps35 accumulated at most double at the protein level, which suggested that only dVps35 incorporated in the retromer complex is stable. Consequently, we expressed the *dVps35* transgenes in the *dVps35* heterozygous or homozygous genetic background to analyze the effects of the PD mutation (Fig. 1A).

It has been reported that dVps35 inactivation increases the number of synaptic boutons of the neuromuscular junction (NMJ) in larval motor neurons (26). A similar synaptic phenotype was reported in *dLRRK* mutant flies (18). Supporting these findings, immunosignals of dVps35 were localized in both the nerve terminals and cell bodies of primary cultured neurons (Supplementary Material, Fig. S1), which was similar to those of dLRRK (14). We tested whether dLRRK modulates changes in the number of synaptic boutons by dVps35 inactivation. As previously reported, dVps35 inhibition led to increased numbers of type Ib synapse boutons, which was suppressed by the introduction of dVps35 WT but not dVps35 DN (Fig. 1C and D) (26). The increase in bouton number was observed by both neuronal and muscular suppression of *dVps35* (Supplementary Material, Fig. S2A and B), while the postsynaptic property of the subsynaptic reticulum (SSR) in the muscles was preserved based on Dlg and GluR2 expression (Supplementary Material, Fig. S2C). However, ultrastructural abnormalities were detected in *dVps35*-deficient SSR, where extramembrane structures appeared in the reticulum lumen

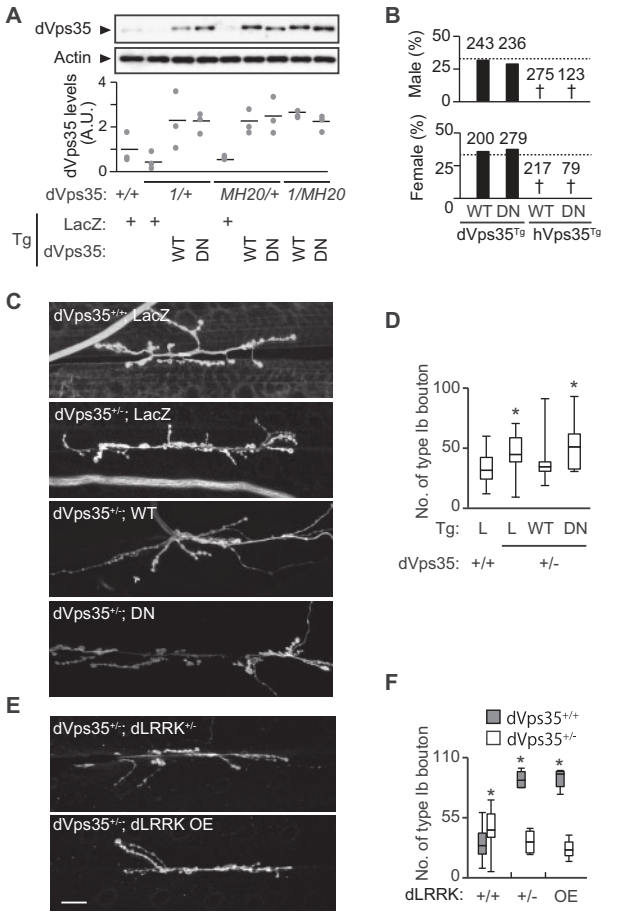

Figure 1. dVps35 and dLRRK regulate synaptogenesis. (**A**) Endogenous *dVps35* expression and transgenic expression (Tg) of *LacZ*, *dVps35* WT and *DN* mutant in the $dVps35^{1}$ or $dVps35^{MH20}$ heterozygous or compound homozygous genetic backgrounds were analyzed in adult heads. LacZ served as a control transgene. Dots represent relative band intensities of dVps35 normalized to actin and dashes represent mean values. $n = 3$ independent experiments. A.U., arbitrary units. (**B**) Eclosion percentages of $dVps35^{-/-}$ flies expressing WT or DN forms of dVps35 or hVps35 by crossing $dVps35^{+/-}$ flies harboring the ubiquitous *Da-GAL4* driver and the indicated UAS transgenes. The total number of offspring obtained by the crosses is indicated in the graph. †, lethal. Expected emergence ratio (33.3%) in accordance with Mendelian laws is indicated by dashed lines. (**C** and **E**) Synaptic morphologies of the NMJs in the larval motor neurons with the indicated genotypes. dVps35 and dLRRK were expressed by the motor neuron-specific *OK6-GAL4* driver. Scale bar, 20 μm. (**D** and **F**) Boxplots represent quantification of the total numbers of type Ib boutons with the indicated genotypes shown in **c** and **e**. L, LacZ; WT, Vps35 WT; DN, Vps35 DN. $n = 7$–20 (**D**), 6–20 (**F**) NMJs in 3-10 flies, $^{*}P < 0.05$ *vs.* $dVps35^{+/+}$; $dLRRK^{+/+}$, Dunnett's test. OE, overexpression.

(Supplementary Material, Fig. S2D). This SSR phenotype appeared to be largely suppressed by dVps35 WT but not DN. Either increased or decreased dLRRK expression caused an increase in bouton number, which was suppressed by the removal of one copy of the *dVps35* gene (Fig. 1E and F). *dVps35*-deficient larvae die at the 3rd instar stage, which suggests that maternal *dVps35* transcripts support their early development. Indeed, specific but reduced vesicular signals of dVps35 were still detected at the boutons of *dVps35*-deficient larvae (Fig. 2A and B, Supplementary Material, Fig. S2E), the size of which was smaller than a normal control (Fig. 2A and C). However, the distribution of dVps35-positive vesicular signals in synapse membrane regions decreased in *dVps35*-deficient larvae. The introduction of dVps35 WT and DN fully rescued the shrunk bouton phenotype, whereas only dVps35 WT facilitated the perimembranous localization of dVps35-positive vesicles (Fig. 2A and D). Approximately, half of dVps35 vesicles localized around the synapse membrane in $dVps35^{+/+}$ animals, and some of them bordered the synaptic release region active zones (AZs) (white arrowheads in Fig. 2A). Although the number of AZs in the terminal boutons was not changed by dVps35 manipulation, ectopic expression of dVps35 WT promotes the localization of dVps35-positive vesicles at AZs (Fig. 2A, E, F). These data suggest that dVps35 and dLRRK are required for NMJ development and that dVps35-containing vesicles partly border on the AZ, whereas the distribution of the vesicles is altered by dVps35 DN mutation.

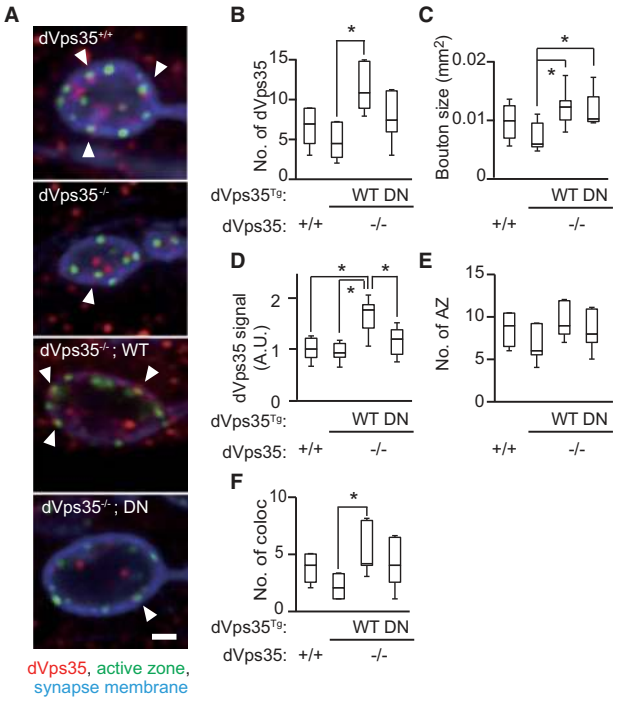

Figure 2. dVps35 is localized in the synaptic boutons. (**A**) Distribution of dVps35 in the distal synapse boutons of the indicated genotypes. dVps35 signals adjacent to the active zones (AZs) are shown (arrowheads). Scale bar, 2 μm. (**B–F**) Boxplots show the number of dVps35 signals in the distal boutons (**B**), the bouton size (**C**), the dVps35 localization ratio in the synapse perimembrane region (within 0.5 μm of membrane, **D**), the number of AZs (**E**) and AZs overlapped with dVps35 (**F**). $n = 5–8$ larvae, $F = 5.74$ (**B**), 4.47 (**C**), 21.01 (**D**), 3.07 (**F**), one-way ANOVA with *post hoc* Tukey-Kramer's test. $^*P < 0.05$. There were no significant differences between $dVps35^{+/+}$ and $dVps35^{-/-}$ in the comparison of four genotypes. Transgenes were driven by the ubiquitous *Da-Gal4*.

dVps35 is involved in SV dynamics

dLRRK is implicated in SV recycling, and the loss of dLRRK increases with the appearance of large SVs and cisternal structures (20). Our above results and recent studies by other groups suggest that dVps35 genetically interacts with dLRRK (11,23), which prompted us to test the possibility that dVps35 also regulates SV dynamics. Ultrastructural analysis of *dVps35*-deficient boutons revealed that SVs decreased in number and increased in size (Fig. 3A and B, Supplementary Material, Fig. S3A). The appearance of cisternal structures also increased in the periactive zones (Fig. 3A and B), which was likely to derive from larger endocytic vesicles (Fig. 3C and D). These SV defects closely resembled those of the *dLRRK* mutant (20). The complementary expression of dVps35 WT but not DN in *dVps35*-deficient flies almost rescued these SV phenotypes (Fig. 3A and B).

To estimate the effects of dVps35 on SV dynamics at the boutons of larval NMJs, synaptic endocytosis activity (Fig. 3E and F) and the SV reserve pool (Supplementary Material, Fig. S3B) were visualized with FM1-43 lipophilic fluorescent dye and a vesicular monoamine transporter (VMAT) with a pH-sensitive fluorescent protein VMAT-pHluorin, respectively. The loss of *dVps35* impaired spontaneous endocytosis at synapse boutons and reduced the amount of SV reserve pools, phenotypes that were rescued by the introduction of dVps35 WT but not DN (Fig. 3E and F, Supplementary Material, Fig. S3B). Conversely, the capacity for SV release was analyzed using VMAT-pHluorin in dopaminergic (DA) neurons in adult brains (Supplementary Material, Fig. S3C) (27). *dVps35* heterozygous mutation and DA neuron-specific *dVps35* knockdown both exhibit defects in SV release (Supplementary Material, Fig. S3C), which were again rescued by the expression of dVps35 WT but not DN (Supplementary Material, Fig. S3C). Taken together, the above results suggested that dVps35 regulates SV dynamics and the PD-associated mutant does not function properly.

Loss of dVps35 affects neurotransmitter release

We next analyzed the electrophysiological properties of muscle 6 of control (*w-*) and *dVps35* mutant 3rd instar larvae. Similar to a previous report on a *dLRRK* mutant, the miniature excitatory junction potential (mEJP) amplitude was increased by loss of *dVps35* (Fig. 4A) (18,20). The larger mEJP amplitude is likely due to the larger SV size, as shown in Figure 3A and B, which would contain more neurotransmitters, or could be due to postsynaptic SSR alterations. Both neuronal and muscular expression of dVps35 WT but not DN successfully suppressed the alteration of the mEJP amplitude similarly to its whole-body complement, which suggested that dVps35 regulates both presynaptic and postsynaptic functions for neurotransmission (Fig. 4B). This idea was further supported by the result that both motor neuron- and muscle-specific knockdown of *dVps35* resulted in increased mEJP (Supplementary Material, Fig. S2B). The quantal content, which represents the amount of neurotransmitter released from presynapses, was decreased in *dVps35* animals (Fig. 4C). In contrast, the amplitude of EJP and the paired pulse ratio of the *dVps35* mutant did not change compared to a normal control, similarly to the *dLRRK* mutant (Fig. 4C) (20).

Given that the lack of dVps35 affects both SV release (Supplementary Material, Fig. S3C) and synaptic endocytosis (Fig. 3E and F), we next performed high-frequency electrical stimulation (5 Hz for 10 min) to analyze SV recycling capacity (Fig. 4D and E). Spike amplitudes were mildly decreased during 10-min stimulations in $dVps35^{+/+}$ larvae, which indicated that SV

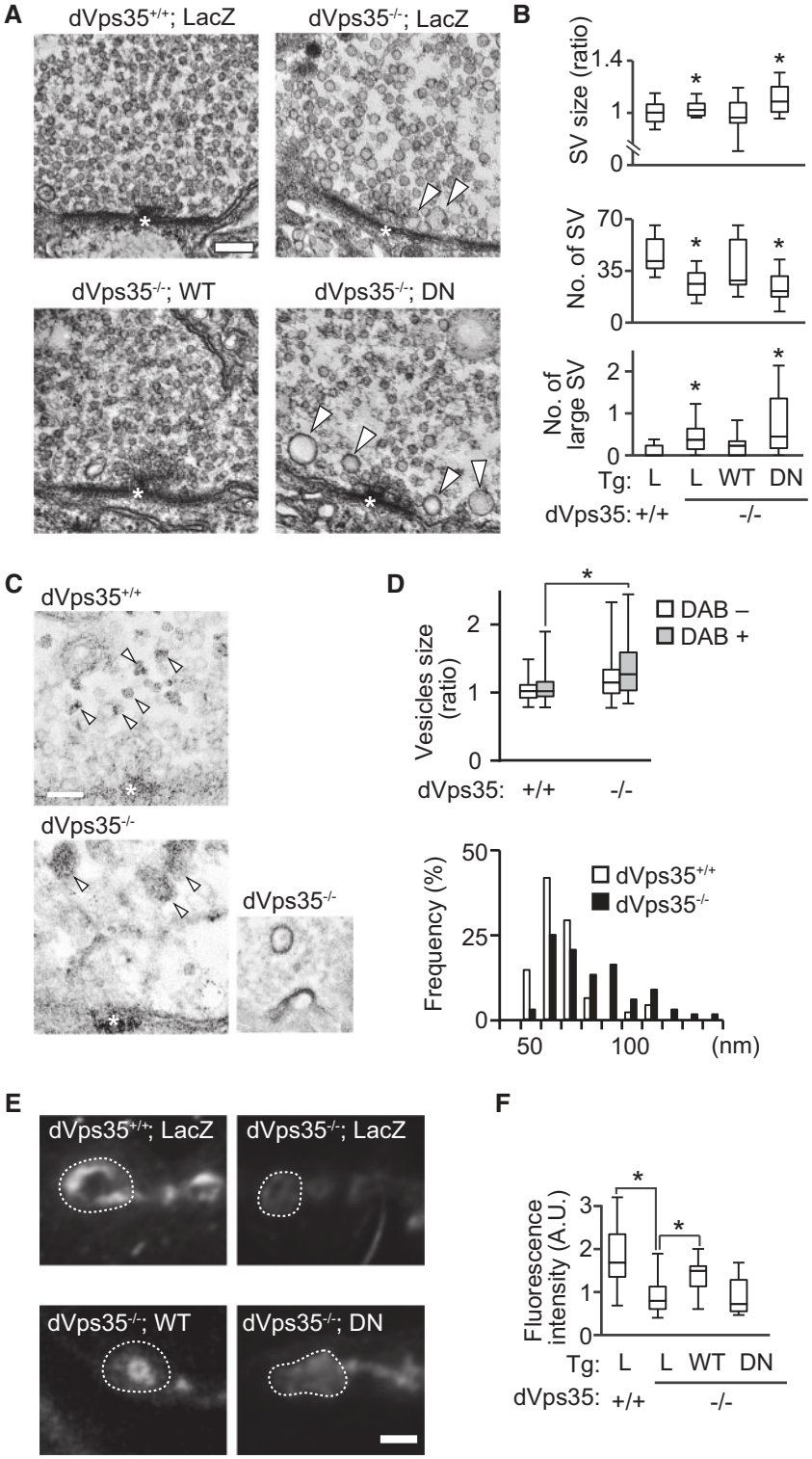

Figure 3. dVps35 is involved in synaptic vesicle endocytosis. (**A**) Ultrastructure of the AZ regions in larval motor neurons with the indicated genotypes. Asterisks and arrowheads indicate AZs and large vesicles (>70 nm in diameter), respectively. Scale bar, 100 nm. (**B**) Quantification of the relative SV size, numbers of SVs and >70-nm vesicles in the unit area (defined in Supplementary Material, Fig. S3A). L, LacZ; WT, Vps35 WT; DN, Vps35 DN. $n = 5–11$ AZ neighboring regions in 3–5 flies, $^*P < 0.05$ *vs.* *dVps35*$^{+/+}$, Dunnett's test (SV size and No. of SV) or Steel's test (No. of large SV). (**C**) Endocytosed vesicles of synaptic boutons labeled with DAB (arrowheads) during 10 min of FM1-43 FX treatment in the presence of 5 mM Ca^{2+}. Large endocytosed vesicles labeled by photoconversion were frequently observed in *dVps35*$^{-/-}$ larvae. Arrowheads and asterisks indicate DAB-positive vesicles and AZs, respectively. Scale bars, 100 nm. (Right) DAB-positive endocytic invagination (arrowheads) observed in *dVps35*$^{-/-}$ larvae. Scale bars, 200 nm. (**D**) The average size of DAB-positive and -negative endocytosed vesicles (upper) and the size distribution of DAB-positive vesicles (lower). $n = 47–67$ vesicles from 8 to 14 synapse boutons in 3 larvae. $^*P < 0.05$, two-tailed *t*-test, $t = 2.25$. (**E** and **F**) Endocytic activity of the distal synapse boutons (marked by dashed lines) in living larvae by pulse-labeled FM1-43 FX fluorescence. Endocytic activity was quantified as fluorescence intensity. $n = 7–15$ synapse boutons in 5–10 flies, $^*P < 0.05$ *vs.* *dVps35*$^{+/-}$, Dunnett's test.

regeneration was achieved effectively. Loss of a copy of *dVps35* caused a larger reduction ratio. The introduction of dVps35 WT at the endogenous level rescued this defect, whereas the introduction of dVps35 DN under the same condition appeared less stable in proteins and did not rescue the EJP reduction of $dVps35^{+/-}$ flies, which indicates that dVps35 DN behaves as a loss-of-function mutation in SV regeneration during high-frequency stimulation (Fig. 4D and E, Supplementary Material, Fig. S4).

dVps35 and dLRRK regulate synaptic endocytosis and SV regeneration through the Rab-mediated endocytic pathway

Because *dVps35* genetically interacts with *dLRRK* in synaptic functions, we next examined the sublocalization of dVps35 and dLRRK at the synapses by immunoelectron-microscopic analysis (Fig. 5A–E). dVps35 immunosignals were distributed at the edges of active zones (Fig. 5A and B), inside the boutons (Fig. 5C) and in the SSR regions (Fig. 5D and E). dLRRK signals were located inside of the boutons and the SSR rather than the plasma membrane compartment, and few dLRRK signals colocalized with dVps35, which suggested that dLRRK and dVps35 cooperate sequentially at different sites to regulate SV dynamics (Fig. 5C and E). dLRRK/LRRK2 regulates Rab5 and Rab11 in *Drosophila* and cultured neurons (16,17,28,29). dVps35 was partially colocalized with Rab5 and surrounded by Rab11 but not Rab9 at the synapses (Fig. 5F). Supporting this observation, hVps35 could associate with Rab5a/b and Rab11a/b, but not Rab7 or Rab8A (Fig. 6A). The affinity of hVps35 for Rab5a/b was similar between WT and DN mutant (Fig. 6B).

Membranes invaginated from the edges of the active zone, which were thought to be endocytic intermediates of SV, were frequently observed in *dVps35*-deficient larvae, implying an endocytic defect of SV (Fig. 5G and H and Fig. 3C). Rab5 regulates SV endocytosis (17,28,30), and the involvement of Rab11 in SV dynamics was supported by altered SV morphology of the NMJs expressing a dominant-negative form of Rab11 (Supplementary Material, Fig. S5). Considering the above findings, we tested whether Rab5 and Rab11 affect the *dVps35* synaptic phenotypes. Rab5 and Rab11 overexpression suppressed the overproliferation of type Ib boutons and restored the SV number of the $dVps35^{-/-}$ larvae (Fig. 7A–C). Rab5, Rab11 and dLRRK overexpression leads to the suppression of the large SV appearance and a reduction in the average SV size, likely due to the promotion of the membrane tubulation and scission processes during SV regeneration (Fig. 7B and C). Notably, the removal of a copy of dLRRK also suppressed the reductions in SV number and large SV appearance, implying a complex relationship between Vps35 and LRRK2 in the balance of their activities and synaptic context (Fig. 7B and C).

The morphological rescue of synapse boutons of the *dVps35* heterozygous larvae by dLRRK, Rab5 and Rab11 overexpression prompted us to test whether the electrophysiological defects of the *dVps35* mutant could be suppressed by the manipulation of these molecules. The manipulation of dLRRK activity in either direction rescued the reduction of sustained neuronal activity of $dVps35^{+/-}$ larvae by high-frequency electrical stimulation (Fig. 7D). Endophilin A (EndoA) is involved in an early event of synaptic endocytosis and regulated by LRRK2-dependent phosphorylation (20,31). *EndoA* overexpression markedly rescued the defects of sustained neuronal activity of $dVps35^{+/-}$ larvae whereas removal of a copy of *EndoA* failed to do so (Fig. 7E). Similarly, Rab11 but not Rab5 or LacZ overexpression markedly rescued it (Fig. 7F and G). In contrast, partial knockdown of Rab5 completely rescued it although Rab5 knockdown in the $dVps35^{+/+}$ genetic background mildly impaired the neuronal activity (Fig. 7H and I). Collectively, these genetic tests suggest that Vps35 contributes to the maintenance of a functional SV pool downstream of *Rab5* in a fine balance with LRRK2 and EndoA activities and that the enhancement of the SV recycling pathway by Rab11 overexpression improves synaptic defects due to *dVps35* loss.

Given that Vps35 maintains a harmonious control with Rab5 and dLRRK in the SV recycling, we next analyzed the neuronal activity-dependent interactions of these molecules using *in situ* proximity ligation assay to detect transient protein-protein interactions. Specific interaction signals between dVps35 and Rab5, which were observed when larvae were incubated with both anti-dVps35 and anti-GFP antibodies, were detected in dVps35 WT-expressing larvae before and after synaptic stimulations (Fig. 8A and B). In contrast, the dVps35 DN and Rab5 interaction tends to decrease before stimulation and almost disappeared after stimulation (Fig. 8A and B), which was not due to the changes of dVps35 levels at synapses (Fig. 8C and D). The interaction signals in axons were observed both in dVps35 WT and DN flies even after stimulation (Fig. 8B, bottom). Similar experiments were performed for dVps35-Rab11 or dVps35-dLRRK interactions (Fig. 8E–G). Rab11 appeared to bind to dVps35 constantly before and after synaptic stimulations while there were no signals of dVps35-dLRRK interactions, which was consistent with the immunoelectron-microscopic observation that dLRRK and dVps35 signals are not colocalized.

The coordinated actions of dVps35 and dLRRK are required for dopaminergic activity and survival

Although the $dVps35^{+/-}$ flies expressing dVps35 DN failed to rescue the short lifespan phenotype of $dVps35^{+/-}$ flies (Fig. 9A), there was no evidence of DA neuronal loss by dVps35 DN expression in the $dVps35^{+/-}$ and $dVps35^{-/-}$ genetic backgrounds (Fig. 9B). We then examined whether the introduction of the *dVps35* mutant allele affects the development and the DA neuron survival in $dLRRK^{-/-}$ flies. The *dLRRK* mutant allele *e03680* was inherited in males at a Mendelian ratio so that ~33% of *dLRRK* homozygous mutants emerged when *e03680* heterozygous mutants balanced over the *TM6B* balancer chromosome were inbred (Fig. 9C). The introduction of the *dVps35* mutant allele *MH20* affected the *dLRRK* emergence ratio, whereby the ratio was reduced to half by the heterozygous introduction of the *dVps35* mutant allele, which was lethal with the homozygous introduction of *dVps35* (Fig. 9C). Given that the concurrent loss of dVps35 and dLRRK activities affected the survival, we next examined whether the introduction of the *dLRRK* mutant allele affected the DA neuron survival in the $dVps35^{+/-}$ background complementarily expressing dVps35 WT or DN (Fig. 9D). The expression of dVps35 WT or DN in the $dVps35^{+/-}$; $dLRRK^{+/-}$ background did not affect DA neuron survival, whereas the loss of DA neurons in $dVps35^{+/-}$; $dLRRK^{-/-}$ flies failed to be rescued by dVps35 WT expression, which was further exacerbated by dVps35 DN (Fig. 9D).

To examine the possibility that DA neuronal functions are disturbed before neuronal death in *dVps35* mutant flies, we examined the sleep and arousal behaviors regulated by DA neuronal function and related to sleep disturbance, one of the known non-motor symptoms of PD (32). Impaired sleep behavior was observed when dVps35 was inhibited in DA neurons using

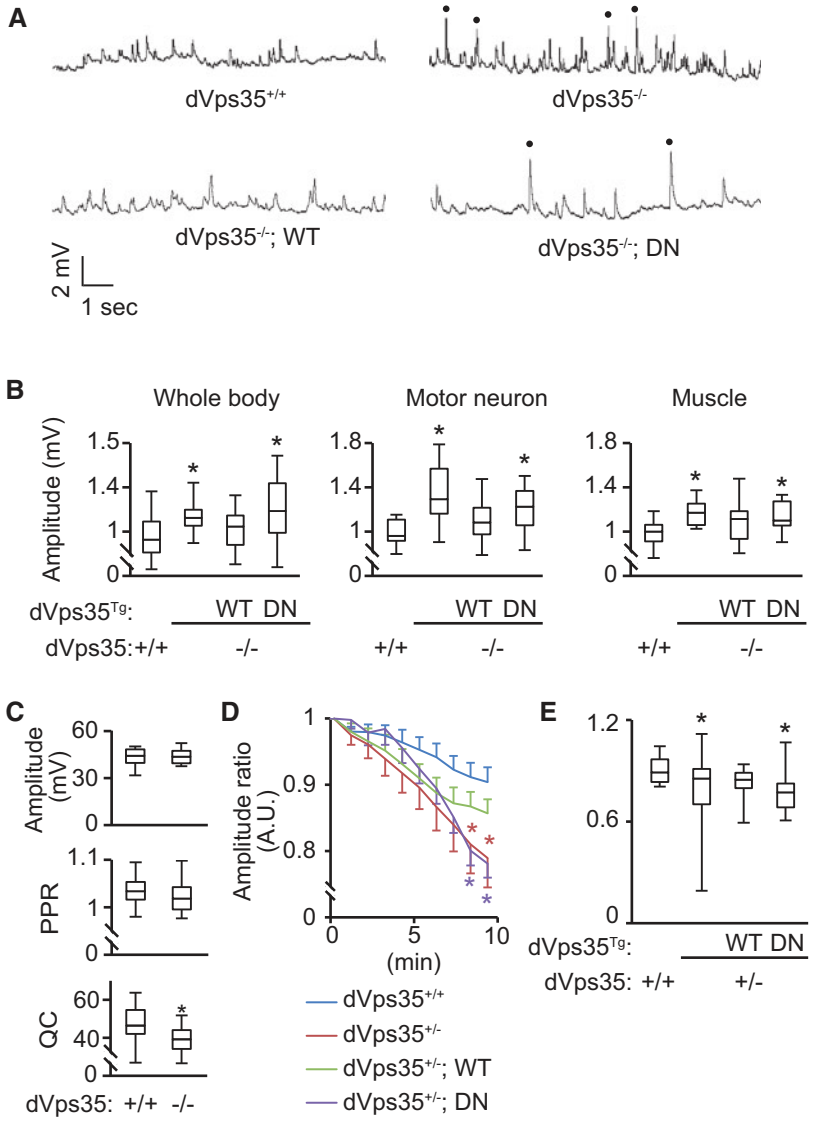

Figure 4. dVps35 mutations affect spontaneous neurotransmitter release. (**A**) Representative spontaneous mEJP traces in the larval NMJ. Black dots indicate large spikes (> 2mV). (**B**) mEJP amplitudes were recorded in larval NMJs with the indicated genotypes in the presence or absence of transgenic dVps35 WT or DN. Transgenes were driven by *Da-GAL4* (Whole body), *D42-GAL4* (Motor neuron) or *MHC-GAL4* (Muscle). Averaged mEJP amplitudes are graphed. $n = 11$-24 (Whole body), 14–21 (Motor neuron) and 9–13 (Muscle) synapse boutons in 6–13 (Whole body), 7–11 (Motor neuron) and 5–7 (Muscle) flies. $^*P < 0.05$ *vs.* $dVps35^{+/+}$, Steel's test. (**C**) EJP amplitudes, paired-pulse ratios (PPRs) and quantal content (QC) were recorded in larval NMJs with $dVps35^{+/+}$ or $dVps35^{-/-}$ genotypes. PPR was graphed as a ratio of EJP amplitudes by paired electrical stimulations (50 ms interval). $n = 12$–20 NMJs in 6–10 flies. (**D**) Average amplitude ratios of every min to the first 1 min (mean ± s.e.m.) by high-frequency stimulation (5 Hz, 10 min) were graphed. (**E**) The relative reduction of the EJP ratio of the last 1 minute in (**D**). (**D** and **E**) $n = 6$–19 larvae, $^*P < 0.05$ *vs.* $dVps35^{+/+}$, Welch's test.

dVps35 RNAi, and a similar sleep phenotype was observed in $dVps35^{+/-}$ flies (Fig. 9E). The reduced sleep behavior of $dVps35^{+/-}$ flies was suppressed by DA neuron-specific expression of dVps35 WT; dVps35 DN further extended the sleep period compared to dVps35 WT (Fig. 9F).

The reduction of sleep behavior in $dVps35^{+/-}$ flies was rescued by DA neuron-specific expression of Rab5, Rab11 and dLRRK while the removal of a copy of the *dLRRK* gene failed to do so (Fig. 9G). Impaired motor ability of $dVps35^{+/-}$ larvae was also rescued by the ubiquitous expression of dLRRK, Rab5 and Rab11 or by the reduction in dLRRK activity (Fig. 9H and I). Again, these results suggest that the manipulation of dLRRK, Rab5 and Rab11 activities counteracts the endocytic hindrance of SVs by reducing Vps35 activity.

Discussion

The identification of the retromer component *dVps35* as a PD-responsible gene has reinforced the idea that dysregulation of membrane dynamics is an important etiology in PD. While Vps35 is ubiquitously expressed as the retromer component, missense mutations of Vps35 lead to late-onset PD. To understand the effects of a PD-associated mutation of Vps35 in neural tissues, we designed the transgenic expression of hVps35 and *Drosophila* orthologues in *Drosophila* under the condition of reduced dVps35 levels, namely in the *dVp35* heterozygous or homozygous genetic background. Despite the fact that Vps35 is highly conserved from yeast to humans, hVps35 did not complement dVps35 functions, which was consistent with a

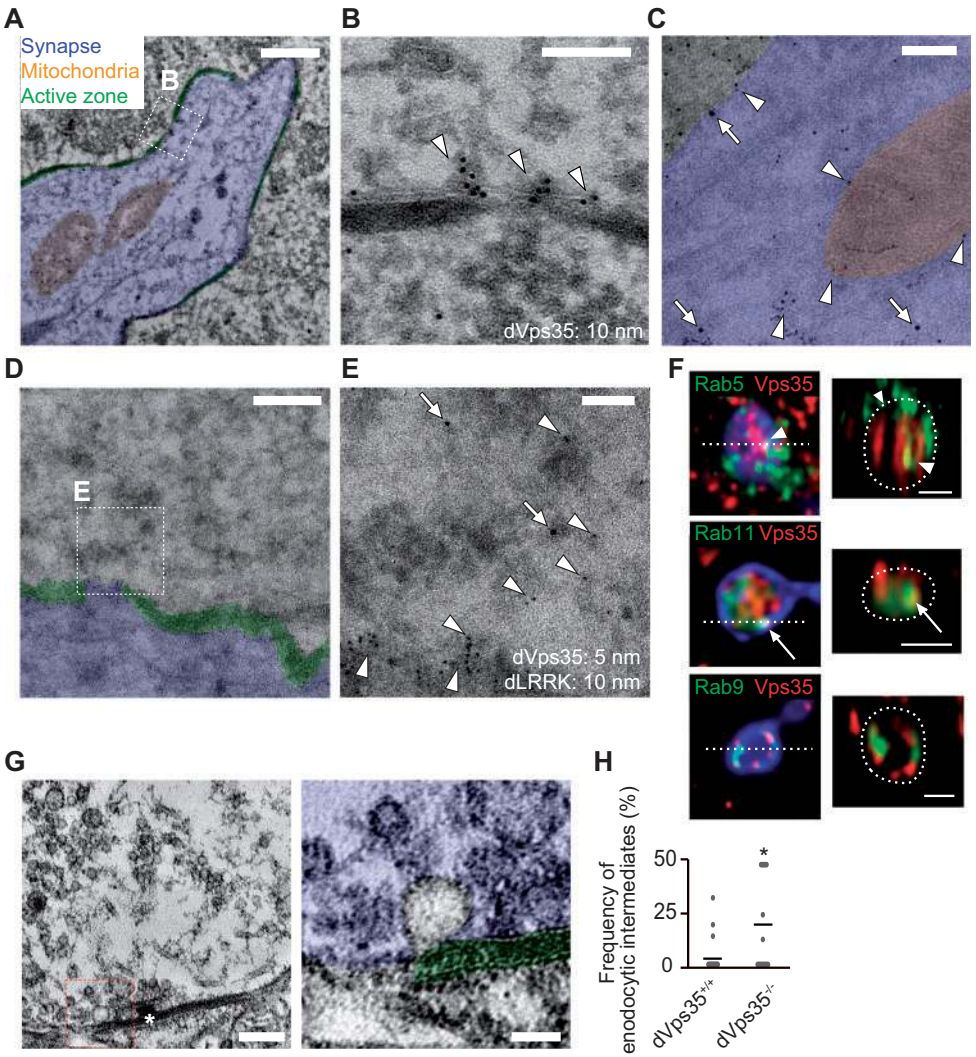

Figure 5. dVps35 is localized in the region of SV endocytosis. (**A-E**) Immunoelectron micrographs showing presynaptic terminals containing AZs (**A** and **B**) and mitochondria (**A** and **C**) and SSR (**D** and **E**). (**B** and **E**) High-magnification images of a boxed region in (**A** and **D**) are shown. (**A** and **B**) Vps35 is labeled by 10-nm gold particles (arrowheads). (**C-F**) Vps35 and dLRRK are labeled by 5-nm (arrowheads) and 10-nm gold (arrows) particles, respectively. Scale bars, 500 nm (**A** and **D**), 50 nm (**B**), 200 nm (**C**), or 100 nm (**E**). (**F**) dVps35, Rab5, Rab9 and Rab11 localizations in the synapse boutons of the NMJs. Z-stack reconstruction images of the positions marked by dashed lines are also shown on the right. Arrowheads and arrows indicate that the dVps35 immunosignal partially overlapped with Rab5 and dVps35 surrounded by Rab11 signals, respectively. Scale bars, 2 μm. (**G**) Ultrastructure of *dVps35*$^{-/-}$ boutons containing AZs (left, asterisk). High-magnification image of a boxed region in the left image shows endocytosed intermediates attached to the membrane compartment in the border between the plasma membrane and AZs (green) (right). Scale bars, 200 (left) and 50 nm (right). (**H**) The frequency of endocytosed intermediates per AZ. $n = 23$-25 AZs in 3 flies, $^{*}P < 0.05$, two-tailed *t*-test, $t = -2.53$.

previous study (33). A dominant-negative function of hVps35 in the retromer complex was also reported in yeast (34). Our findings led us to caution others about the interpretation of the previous results using hVps35 transgenic fly models (33,35).

Vps35-linked PD is inherited as a dominant trait, which may imply that the Vps35 DN mutation has a gain-of-function toxicity. However, dVps35 DN overexpression did not exhibit DA neuron loss throughout the lifespan and acted as a loss-of-function allele in synaptic phenotypes, including morphological features of synaptic boutons, phenotypes of SV dynamics and electrophysiological properties when expressed in *dVps35* heterozygous or a homozygous genetic background, consistent with previous reports (33,36,37). Yet, dVps35 DN rescued the lethality of *dVps35* null flies, suggesting that dVps35 DN is largely functional except for coordinated neuronal functions and synaptogenesis (33,38). A similar conclusion has been obtained in Vps35 DN knock-in mice (37).

Our genetic analysis combined with histochemical and electrophysiological approaches revealed that dVps35 in cooperation with dLRRK regulates SV endocytosis in addition to synaptogenesis. dVps35 immunosignals were mainly condensed in the edges of AZ and in the electron-dense region (likely corresponding to the plasma membrane) of the postsynaptic SSR in NMJs, while dLRRK immunosignals were localized inside of the boutons and in the SSR more dispersedly, which provided evidence of differences between dVps35 and dLRRK in terms of their molecular roles. Consistent with the above findings, dVps35-dLRRK-binding signals were negative in the proximity ligation assay (PLA) of this study and hVps35 did not interact with human LRRK2 in our immunoprecipitation assay (data not shown).

There are several possible causes of increased mEJP amplitude after *dVps35* loss. An increase in the number of synapse boutons after *dVps35* loss could contribute to an increased

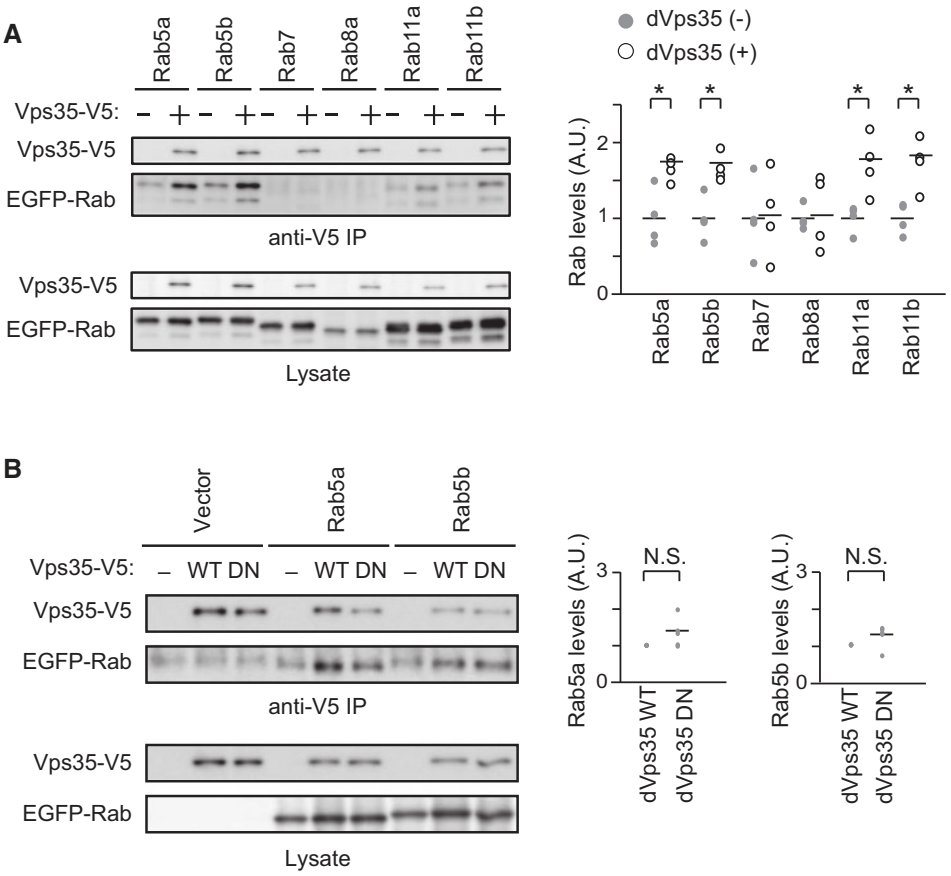

Figure 6. Interaction of Vps35 with Rab GTPase. (**A**) Vps35 interacts with a series of Rab GTPases. Lysate of HEK293T cells expressing EGFP-tagged Rabs with or without hVps35 with a V5 tag were immunoprecipitated with anti-V5 antibody (anti-V5 IP). Coprecipitated Rab proteins were detected with anti-GFP. Graph represents relative band intensities of Rab proteins normalized to each input in the presence (+) or absence (-) of Vps35-V5 and lines represent mean values. $n = 4$ independent experiments. *$P < 0.05$, two-tailed t-test, $t = 3.29$ (Rab5a), 3.90 (Rab5b), 3.31 (Rab11a), 3.76 (Rab11b). (**B**) Both Vps35 WT and DN bound to Rab5a and Rab5b with similar affinity. Graphs represent relative band intensities of co-precipitated Rab5a or Rab5b normalized to dVps35 WT or DN and lines represent mean values. $n = 5$ independent experiments. N.S., not significant by two-tailed t-test.

probability of neurotransmitter release, while an increase in SV size by *dVps35* loss may release more neurotransmitters at once. Increased sensitivity in the postsynaptic field could also account for this phenotype because the lumenal architecture of the SSR was changed by *dVps35* loss, albeit without significant alteration of GluR2 or Dlg expression. The observation that presynaptic- or postsynaptic-specific inactivation of *dVps35* exhibited the same mEJP phenotype suggests the contribution of the above factors to this phenotype, even though presynaptic inactivation showed a stronger phenotype.

Rab5 and Rab11, in addition to dLRRK, also regulate SV endocytosis and recycling (20,39), and involvement of dLRRK/LRRK2 in Rab5 and Rab11 regulation is also possible in *Drosophila* and rat cultured neurons (16,17). The manipulation of these activities improved the decline of high frequency stimulation-mediated neurotransmission in $dVps35^{+/-}$ larvae. Considering the observation that the overexpression of Rab11 but not Rab5 rescued the neurotransmission defects by *dVps35* loss, dVps35 could be involved upstream of Rab11. While Rab5 is implicated in SV endocytosis, Rab11 is proposed to regulate the budding of SV from the synaptic endosomes to regenerate SVs, although it remains unclear whether dVps35 functions along with Rab11 in the synaptic endosomes (39). In contrast, reduced Rab5 activity or alteration of dLRRK activities ameliorated neurotransmission defects by *dVps35* loss. Considering the previous report that both increased and decreased Endophilin A (EndoA) phosphorylation by dLRRK/LRRK2 impedes synaptic vesicle endocytosis, appropriate activation/inactivation cycles of Rab5 and dLRRK kinase and their balance might ensure efficient SV regeneration linked to endocytosis (20). In this context, overexpressed or inactivated dLRRK slows down the EndoA-mediated endocytosis, which could suppress defects of the subsequent transport steps caused by reduced dVps35 activity in synchronization (Fig. 10). The overexpression of EndoA, which regulates membrane scission along with Dynamin (40), suppressed defects in high frequency stimulation-mediated neurotransmitter release by *dVps35* loss while reduced EndoA activity exacerbated this phenotype. The observation suggests that EnodA is also involved in LRRK2-Rab5-Vps35-independent endocytic pathway (40).

We propose that dVps35 regulates SV endocytosis and regeneration in collaboration with dLRRK, Rab5 and Rab11 based on three pieces of evidence. First, the endocytic intermediates on the edges of AZ (Fig. 5G and H) and 80–90 nm 3, 3'-diaminobenzidine (DAB)-positive vesicles (Fig. 3C), which is likely to be the synaptic endosomes to regenerate SVs (41), were frequently observed in *dVps35*-deficient synaptic boutons even under a steady-state condition, suggesting that the speed of endocytosis is reduced, and the activities of synaptic neurotransmitter release (Supplementary Material, Fig. S3C) and endocytosis

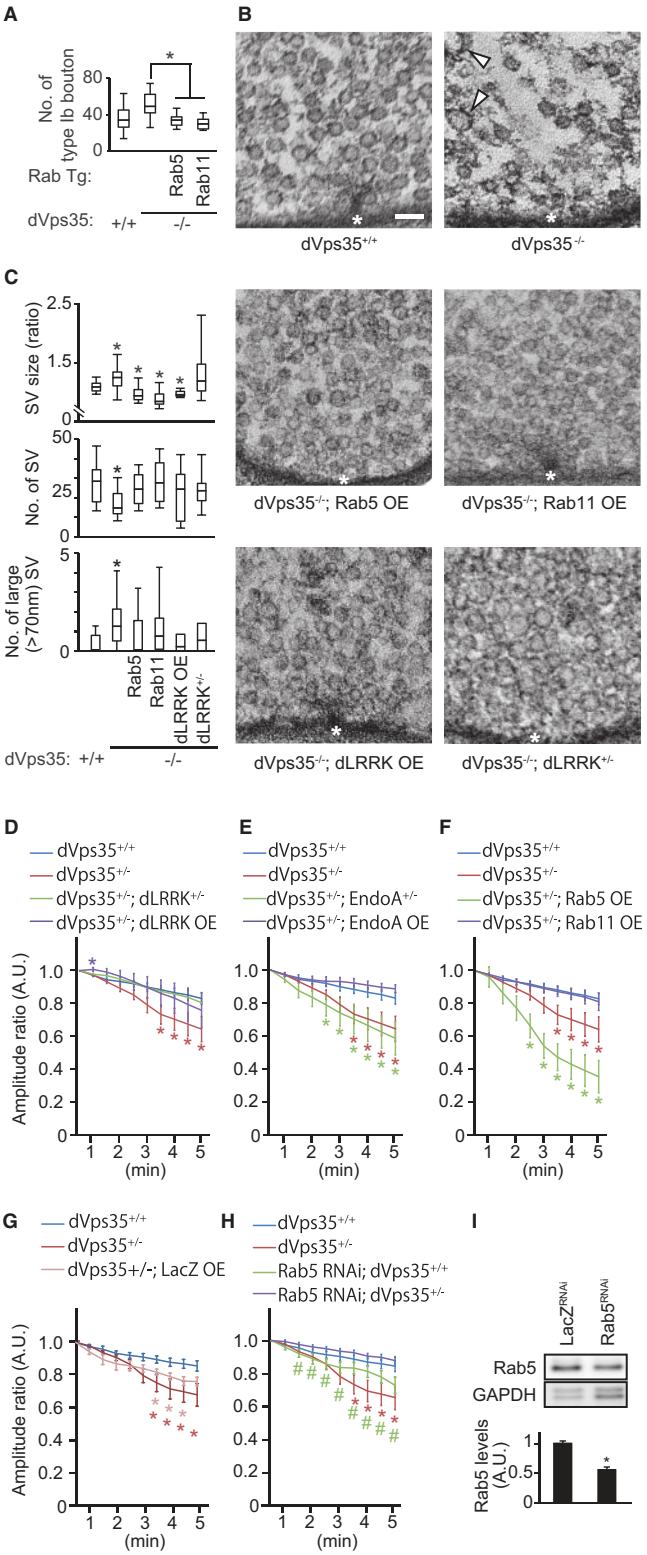

Figure 7. dLRRK, Rab5 and Rab11 are involved in dVps35-mediated synaptic function. (**A**) Total numbers of type Ib boutons in the indicated genotypes. $n = 9$–20 NMJs in 5–10 flies, $^*P < 0.05$ *vs.* $dVps35^{+/-}$, Steel's test. (**B**) Ultrastructure of the AZ regions (asterisks) in the larval motor neurons with the indicated genotypes. Arrowheads indicate large vesicles (>70 nm in diameter). Scale bar, 100 nm. (**C**) Quantifications of the relative SV size, the numbers of SVs and >70-nm vesicles as in Fig. 3B. $n = 5$–11 boutons from 3-5 flies, $^*P < 0.05$ *vs.* $dVps35^{+/+}$, Dunnett's test. (**D-H**) Average amplitude ratios of every 30 s to the first 30 s (mean ± s.e.m.) by high-frequency stimulation (10 Hz, 5 min) were graphed. $n = 3$-12 NMJs in 3-8 flies, $^*P < 0.05$ by two-tailed *t*-test *vs.* $dVps35^{+/+}$, # $P < 0.05$ by two-tailed *t*-test *vs.* $Rab5^{RNAi}$; $dVps35^{+/-}$. $t = 2.32$, 2.21, 2.35, 2.35 ($dVps35^{+/-}$), -2.26 ($dVps35^{+/-}$; dLRRK OE), 3.08, 2.77, 2.59, 2.39, 2.41, 2.25 ($dVps35^{+/-}$; $EndoA^{+/-}$), 3.42, 4.52, 4.81, 4.63, 4.57, 4.65 ($dVps35^{+/-}$; Rab5 OE), 2.35, 2.38, 2.44 ($dVps35^{+/-}$; LacZ), -2.22, -2.14, -2.55, -2.64, -2.43, -2.31, -2.77, -2.72 ($dVps35^{+/-}$; $Rab5^{RNAi}$). (**I**) Endogenous levels of Rab5 protein in control LacZ and Rab5 RNAi flies. Rab5 levels normalized with the intensity of GAPDH were graphed. $n = 3$–5 larvae, $^*P < 0.05$ by two-tailed *t*-test.

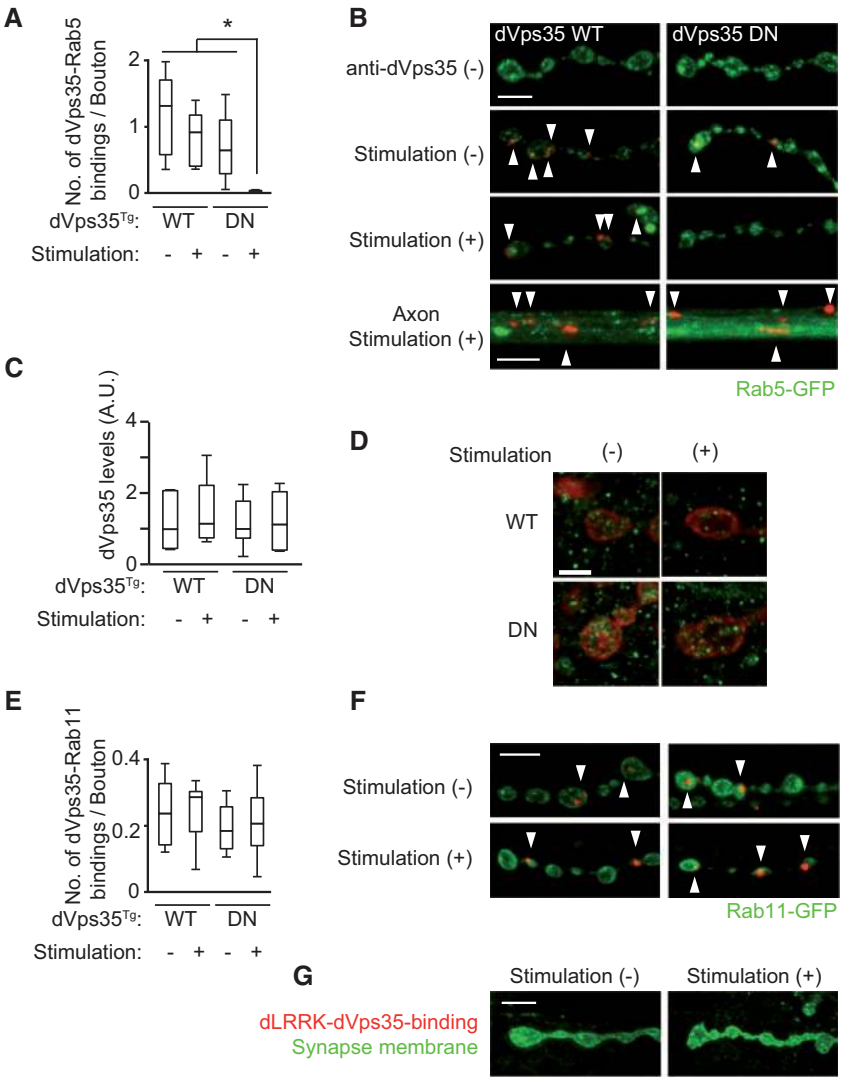

Figure 8. Synaptic activity-dependent dissociation of the PD-associated dVps35 mutant from Rab5. (**A**) Number of dVps35-Rab5-binding signals obtained by a PLA in each bouton of the NMJs before and after synaptic stimulation. (**B**) Representative PLA images (red, arrowheads) of the NMJs and the axons by using anti-dVps35 alone (anti-dVps35) or a combination of anti-dVps35 and anti-GFP antibodies with (+) or without (-) photostimulation in Channelrhodopsin-2-XXL (ChR2)-XXL, Rab5-GFP (green) and dVps35 WT or DN-expressing larvae. (**C** and **D**) dVps35 signals (green) in the distal synapse boutons (red). Larvae were treated as in **A**. Average signal intensities of dVps35 in the distal synapse boutons were not different among samples. Scale bar, 5 μm. $n = 7–10$ synapse boutons from 3 larvae. (**E**) Number of dVps35-Rab11-binding signals in each bouton of the NMJs. (**F**) Representative PLA images (red, arrowheads) in ChR2-XXL, Rab11-GFP (green) and dVps35 WT or DN-expressing larvae. (**G**) Representative PLA images in ChR2-XXL, dLRRK-Myc and dVps35 WT or DN-expressing larvae. Synaptic membranes were visualized with anti-HRP DyLight649 (green). There are no PLA signals. $n = 6–8$ NMJs in 5 flies, $^*P < 0.05$, Steel-Dwass's test. Scale bars = 5 μm.

(Fig. 3E and F) were functionally impaired in *dVps35* mutant flies (42). Second, *dVps35*-deficient flies had large SVs with cisternal endosomal structures (Fig. 3A–D), similarly to *Rab5*-deficient or *dLRRK*-deficient flies (20,28), and the SV phenotypes were rescued by dLRRK, Rab5 or Rab11 manipulation (Fig. 7). Third, dVps35 was colocalized with Rab5 and Rab11 at synapses (Fig. 5F) and hVps35 was associated with Rab5a/b and Rab11a/b (Fig. 6), which are enriched in the SV fraction from rat brain (43).

Dysfunction and subsequent degeneration of nerve terminals are commonly observed in a variety of neurodegenerative diseases. To the best of our knowledge, this is the first study to reveal the molecular roles of Vps35 in the presynapses, where Vps35 DN behaves as a loss-of-function mutant, showing synaptic activity-dependent dissociation of Vps35 DN from Rab5. Supporting our findings, Vps35 DN homozygous knock-in mice exhibit impaired striatal dopamine release stimulated by potassium (37). Increases in the genetic analyses of familial PD cases have led to the identification of causative gene mutations and risk loci, which include *a-Synuclein, LRRK2, Vps35, DNAJC13, Auxilin, Synaptojanin 1, GAK, Vps13c* and *TMEM230* (44,45). These findings suggest that alteration of membrane dynamics is a key element of PD etiology. Focusing on whether these gene functions converge with particular events of membrane dynamics, including SV endocytosis and regeneration, in a DA neuron-specific context is warranted.

Materials and Methods

Drosophila genetics

Fly cultures and crosses were performed on standard fly food containing yeast, cornmeal and molasses, and the flies were

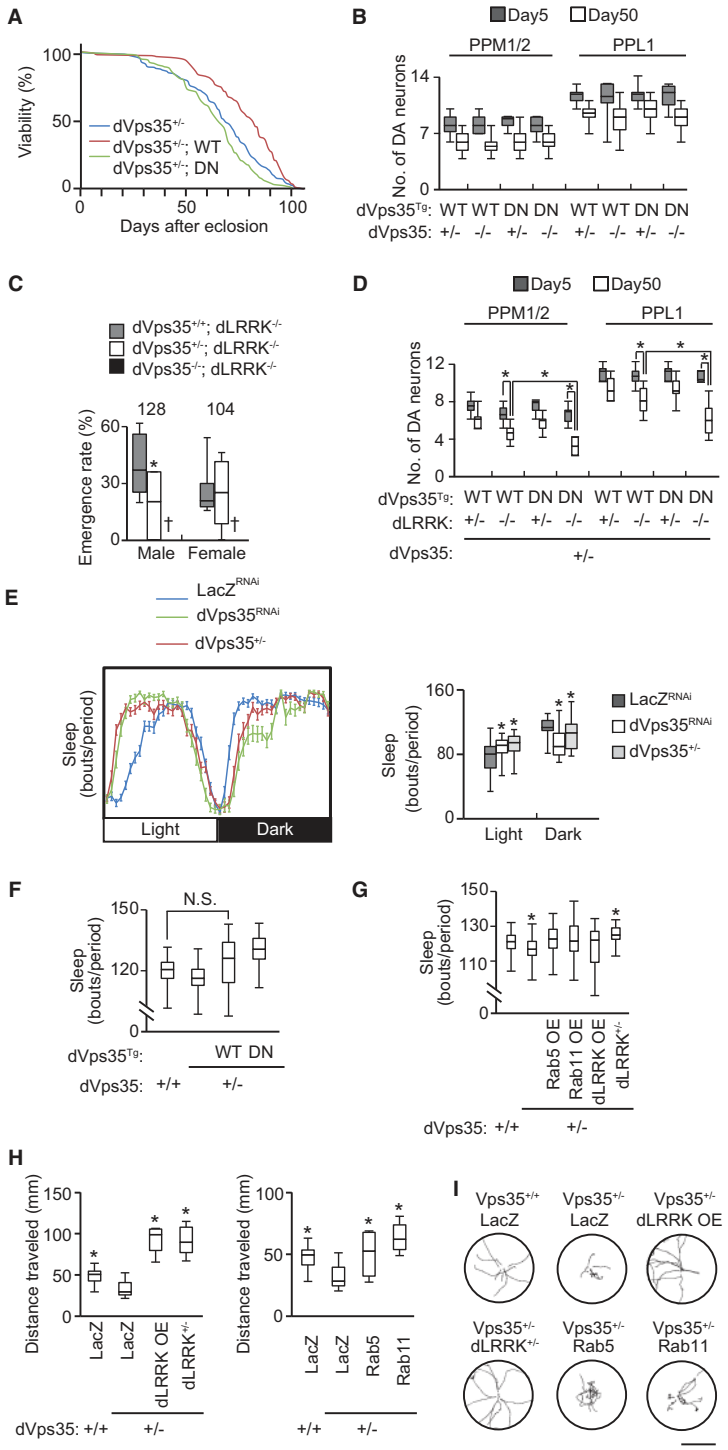

Figure 9. Manipulation of the SV endocytic pathway rescues defects of neuronal activity by *dVp35* loss. (**A**) Lifespan analysis of flies with the indicated genotypes. $n = 250$ ($dVps35^{+/-}$), 151 ($dVps35^{+/-}$; *WT*), 157 ($dVps35^{+/-}$; *DN vs.* $dVps35^{+/-}$). $P < 0.0001$ ($dVps35^{+/-}$; *WT vs.* $dVps35^{+/-}$), $P < 0.0001$ ($dVps35^{+/-}$; *DN vs.* $dVps35^{+/-}$; *WT*), Log-rank test. (**B**) The numbers of PPM1/2 and PPL1 cluster TH-positive neurons were estimated in 5- and 50-day-old adult flies with the indicated genotypes. $n = 10$–17 flies. No significance was noted among age-matched groups by one-way ANOVA. (**C**) Emergence rate of offspring by crossing $dVps35^{+/-}$; $dLRRK^{-/-}$ flies. Note that $dVps35^{+/+}$; $dLRRK^{-/-}$ female flies exhibit a more reduced ratio than expected, which was not affected by the removal of a copy of *dVps35*. $^*P < 0.05$ *vs.* $dVps35^{+/+}$; $dLRRK^{-/-}$, Dunnett's test. The total number of offspring obtained by the crosses is indicated in the graph. †, lethal. (**D**) The numbers of PPM1/2 and PPL1 cluster TH-positive neurons were estimated in 5- and 50-day-old adult flies with the indicated genotypes. $n = 10$ flies, $F = 22.79$ (PPM1/2), 11.84 (PPL1), one-way ANOVA with *post hoc* Tukey-Kramer's test. $^*P < 0.05$. (**E**) Sleep profiles over 3 days in the 12-h light:dark cycle condition are shown in $LacZ^{RNAi}$, $dVps35^{RNAi}$ and $dVps35^{+/-}$ flies (left). The amounts of sleep in the light and dark periods are graphed. $n = 16$–32 flies, $^*P < 0.05$ *vs.* $LacZ^{RNAi}$, Steel's test. (**F**) Daily sleep behaviors of flies with the indicated genotypes. Transgenes were expressed by *TH-GAL4*. $n = 9$–32 flies, N.S., not significant according to Steel-Dwass test and other comparisons have significant differences ($P < 0.05$). (**G**) Daily sleep behaviors of flies with the indicated genotypes. $n = 8$–31 flies, $^*P < 0.05$ *vs.* $dVps35^{+/+}$, Dunnett's test. Note that the $Vps35^{+/+}$ and $Vps35^{+/-}$ data in **F** are presented here to facilitate comparison across genotypes. Data in **F** and **G** were recorded at the same time. (**H**) Moving distance of 3rd instar larvae during 2 min. $n =$ 8–11 larvae each, $^*P < 0.05$ *vs.* $dVps35^{+/-}$; *LacZ*, Dunnett's test. (**I**) Moving tracks recorded over 2 min for the indicated genotypes. Scale bar = 50 mm.

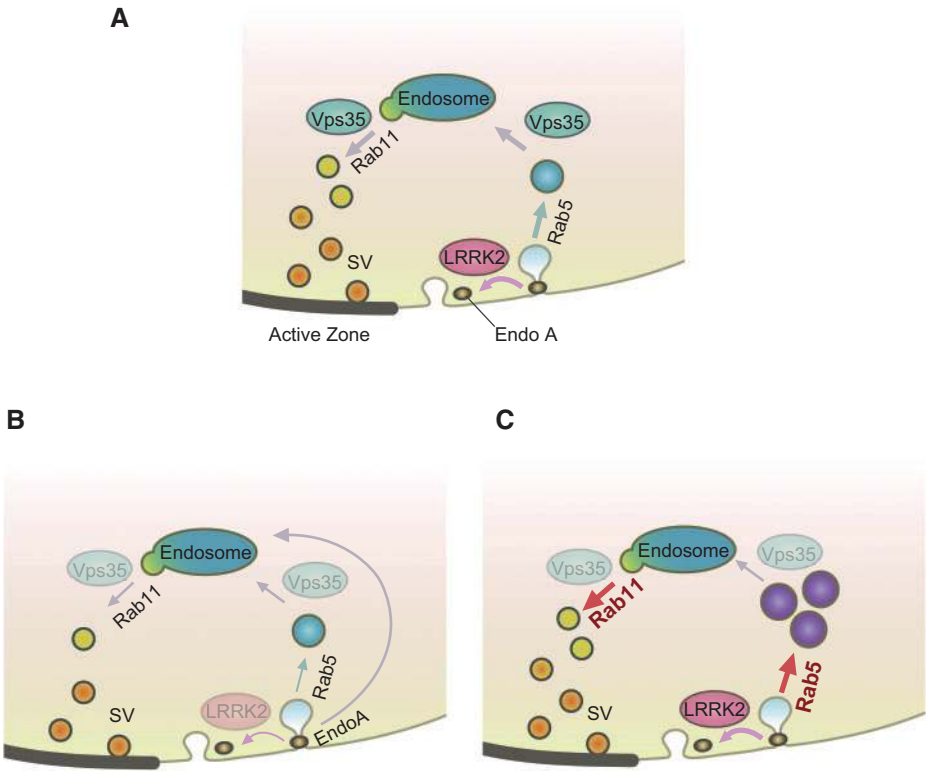

Figure 10. Working hypothesis of the functions of dLRRK, Rab5 and Rab11 in SV dynamics. (**A**) Diagram of dVps35 in the SV dynamic regulation. dLRRK in cooperation with EndoA regulates membrane retrieval from the synaptic membrane after SV fusion to the AZ. dVps35 in cooperation with Rab5 regulates the formation of vesicles from the endocytosed membrane and transports the vesicles to the endosome-like structures (Endosome). After that, dVps35 in cooperation with Rab11 enhances SV budding from the endosome-like structure, regenerating SVs. (**B**) dLRRK overexpression or removal slows down EndoA-mediated membrane retrieval from the synaptic membrane, which facilitates coordination to the subsequent endocytosis step impaired by reduced dVps35 activity by synchronization. EndoA is also involved in a LRRK2-Rab5-Vps35-independent endocytic pathway, which is suggested by an observation that EndoA overexpression but not EndoA$^{+/-}$ suppressed the defects of Vps35$^{+/-}$ in high frequency stimulation. (**C**) Rab5 overexpression promotes the transport of endocytosed vesicles to the endosome-like structures, which is perturbed by reduced dVps35 activity under a condition that induces rapid endocytic retrieval of SVs by a strong stimulus such as high frequency stimulation, while Rab11 overexpression enhances SV budding from the endosome-like structures downstream of a step impaired by reduced dVps35.

raised at 25 °C. The w^{1118} (w^{-}) line was used as a wild-type genetic background. Complementary DNA (cDNA) for *Drosophila* Vps35 (dVps35, provided by Drs. V.I. Korolchuk and C.J. O'Kane) (26) and hVps35 (provided by Dr. M. Farrer) (36) were subcloned into the *pUAST* vector, and *UAS-dVps35 and hVps35* transgenic lines were generated in the w^{-} background. $dVps35^{MH20}$ or $dVps35^{1}$ was used as a null mutant allele of *dVps35*. All other fly stocks and *GAL4* lines used in this study were obtained from the Bloomington *Drosophila* Stock Center, the Kyoto Stock Center, the FlyORF, and the Vienna *Drosophila* RNAi Center and have been previously described: $dVps35^{MH20}$ (25); $dVps35^{1}$ (46); *UAS-dLRRK WT* and $dLRRK^{e03680}$ (14); *dLRRK-Myc* genomic rescue line (47); $dLRRK^{1}$ (15); *UAS-VMAT-pHluorin* (48); *EGFP-Rab5* knock-in line (49); *UAS-dRab5 S43N* (50); *UAS-EGFP-WASH*; *UAS-RFP-Rab9* (51) and *UAS-dParkin* (27). Full details of *Drosophila* genotypes used in this study are described in Supplementary Material, Text S1.

Antibodies and plasmids

Rabbit anti-dVps35 polyclonal antibody was raised against recombinant His-GST-tagged dVps35 (form a, 687-803aa) produced in the *E. coli* strain BL21 harboring pCold II-GST-dVps35. The antibodies used in the western blot analysis were as follows: anti-dVps35 (1:10,000), anti-V5 (1:5,000, Thermo Fisher Scientific, 46-0705), anti-GFP (1:1,000, Abcam, ab6673), anti-Rab5 (1:1,000, Abcam, ab31261), anti-dParkin (1:3,000, in-house) (27), anti-GAPDH (1:1,000, Bioss, 3E12), and anti-α-tubulin (1:5,000, Sigma-Aldrich, DM1A). The antibodies used in immunocytochemistry were anti-*Drosophila* Tyrosine hydroxylase (TH, 1:250, in-house) (14), anti-dVps35 (1:250), anti-Bruchpilot (1:10, Developmental Studies Hybridoma Bank (DSHB), nc82), anti-Myc (1:10, Santa Cruz Biotechnology, 9E10), anti-GluR2A (1:10, DSHB, 8B4D2), anti-Dlg (1:250, DSHB, 4F3), anti-Rab5 (1:100, Abcam, ab31261), anti-GFP (1:200, Wako, 102-20461) and Alexa Fluor594- (1:200) or DyLight649- (1:500) conjugated anti-horseradish peroxidase (HRP) (Jackson ImmunoResearch, 123-585-021 and 123-495-021). The mammalian expression plasmid encoding hVps35-V5 was a kind gift from Dr. M. Farrer, and plasmids for EGFP-Rab GTPases were described elsewhere (16).

Western blot analysis

Fly heads were directly homogenized in 20 μl of 3x SDS sample buffer per head using a motor-driven pestle. After centrifugation at 16,000 × *g* for 10 min, the supernatants were subjected to western blotting.

Lifespan assay and locomotor and sleep behavior assays

For the lifespan studies, approximately 20 adult flies per vial were maintained at 25 °C, transferred to fresh fly food and

scored for survival every 2 d. To control for isogeny, the *Da-GAL4* driver line was backcrossed to the w^- wild-type background for six generations. All *dVps35* transgenic, knockdown and mutant flies were generated in or backcrossed to the w^- genetic background and thus have matched genetic backgrounds.

Sleep and locomotor behaviors were recorded in an incubator (MIR-254, Panasonic Healthcare) using the *Drosophila* Activity Monitoring system (Trikinetics), which monitors the activity of individual flies in polycarbonate tubes (length, 65 mm; inside diameter, 3 mm). Sleep was defined as a bout of 5 or more minutes of inactivity. Behavior of single male flies preconditioned at 25°C under a 12-h light:dark cycle condition for 3 days was individually recorded (16 to 32 flies per experiment) for another 3 days. Daily sleep time was calculated with ActogramJ (http://actogramj.neurofly.de/) and pySolo (https://www.pysolo.net/).

Larval motility

Third instar larvae were placed on the center of 2% agar plate. Larval movements were recorded at 20 fps using a webcam (Buffalo, BSW20KM11BK) and each 5 sec position of larvae were traced by ImageJ software. Moving distance during 2 min was analyzed with MTrack2 plugin of ImageJ software.

Immunostaining and transmission electron microscopy (TEM) analysis

The visualizations of synapse boutons, dVps35 and AZs in larval motor neurons were analyzed by whole-mount immunostaining as previously described (18). Synapse bouton counting and signal colocalization were calculated using Imaris software (Pitplane) and ImageJ software. Immunoelectron microscopy (IEM) using ultrathin cryosections was performed as previously described (52). Briefly, larvae fixed by immersion in 0.1 M phosphate buffer (pH7.2) containing 4% paraformaldehyde (PFA) at 4 °C overnight were immersed in 2.3 M sucrose in PB overnight and plunged into liquid nitrogen. Approximately 60-nm thick sections cut with a cryo-ultramicrotome (UC7/FC7, Leica) were incubated with rabbit anti-dVps35 (1:10) and mouse anti-Myc (1:10) at 4 °C overnight and then with donkey anti-rabbit IgG and anti-mouse IgG conjugated with colloidal gold particles (Jackson) for 1 h. TEM and IEM images were obtained using an electron microscope (Hitachi, HT7700).

FM1-43 dye imaging

Living 3rd instar larvae were dissected in Ca^{2+}-free HL-3 (pH 7.2) solution and incubated for 5 min in HL-3 containing 5 μM FM1-43FX (Thermo Fisher Scientific) and 90 mM KCl. Larvae were then washed with Ca^{2+}-free HL-3 three times, and FM1-43FX fluorescence incorporated into the synapse boutons was measured using a laser-scanning microscope system (TCS-SP5, Leica).

Labeling of endocytosed vesicles by photoconversion

Living 3rd instar larvae were dissected in Ca^{2+}-free HL-3 (pH 7.2) solution and incubated for 10 min in HL-3 containing 10 μM FM1-43 FX in the presence of 5 mM Ca^{2+}. Larvae were then fixed with 2.5% glutaraldehyde in phosphate buffered saline (PBS) for 15 min, washed with PBS three times and incubated with 100 mM ammonium chloride for 10 min. After washing with PBS three times, larvae were pre-incubated in DAB (1.5 mg/ml in PBS) for 10 min, and illuminated under UV light through a 16x objective from a 130 W mercury lamp for 40 min. Preparations were washed with PBS three times and TEM images were obtained using an electron microscope (Hitachi, HT7700).

VMAT-pHluorin live imaging

VMAT-pHluorin live imaging was previously described (27). Briefly, the DA release rates of neuronal fibers and terminals in the whole brain region without the subesophageal ganglion were calculated by normalizing the data with the fluorescence intensity just after photobleaching using ImageJ software.

Electrophysiology

Third instar larvae were dissected in HL-3, and EJPs and mEJPs from NMJs were recorded using an electrophysiological setup equipped with Eclipse FN1 microscope (Nikon), a Multiclamp 700B amplifier (Molecular devices) and a Digidata 1550A data acquisition system (Molecular Devices). Dissected larvae were incubated in HL-3 containing 2.5 mM (for EJP) or 0.375 mM (for mEJP) Ca^{2+}, and a recording electrode filled with 3 M KCl was inserted into muscle 6 of the A3 or A4 segment containing NMJs. All data were analyzed using Mini-Analysis software (Synaptosoft). Quantal content was calculated as mean EJP amplitude divided by mean mEJP amplitude as previously described (18). High-frequency electrical stimulations (5 or 10 Hz) were performed for 5 or 10 min to analyze the reduction ratio during stimulations.

Immunoprecipitation

HEK293T cells, the source of which was described elsewhere (53), were maintained at 37 °C with a 5% CO_2 atmosphere in Dulbecco's modified Eagle's medium (DMEM, Sigma-Aldrich) supplemented with 10% fetal calf serum (FCS, Gibco), GlutaMax (Gibco), non-essential amino acids (Gibco), and 1% penicillin-streptomycin. The plasmids were transfected using Lipofectamine 2000 reagent (Thermo Fisher Scientific) according to the manufacturer's instructions. The total amount of transfected cDNA was adjusted with vector DNA in every transfection experiment. All cells used in these experiments tested negative for mycoplasma contamination.

HEK293T cells expressing EGFP-Rab with or without VPS35-V5 were lysed in RIPA buffer (20 mM Tris-HCl, pH7.4, 150 mM NaCl, 1% NP-40, 0.1% SDS, 2 mM EDTA, and Complete protease inhibitor cocktail (Sigma-Aldrich)). The soluble fraction was subjected to immunoprecipitation with anti-V5 antibody at 4 °C overnight. The antibody–antigen complex was retrieved by the incubation of the lysate with Protein G Dynabeads (Thermo Fisher Scientific) for 2 h at 4 °C. Immunoprecipitates were washed with RIPA buffer containing 200 mM NaCl three times, eluted with 3x sample buffer (150 mM Tris-HCl, pH 6.8, 30% glycerol, 6% SDS, 10% 2-mercaptoethanol) and analyzed by western blotting.

PLA

Third instar larvae expressing *ChR2-XXL* and genes of interest were dissected in HL-3 containing 2 mM Ca^{2+} and incubated for 10 min with or without light pulse stimulations by a 470 nm light emitting diode (16 μW/mm^2, 10 Hz). Larvae were fixed with 4% PFA in PBS and washed with 0.1% Triton-X 100 containing

PBS three times. Preparations treated with immunoreaction enhancer (Can Get Signal immunostain solution A, TOYOBO) for 30 min were further incubated with anti-GFP (1:200) and anti-dVps35 (1:500) overnight at 4 °C. PLA were performed by using Duolink kit (Sigma-Aldrich) according to a manufacturer protocol except for employing a more stringent wash condition of 10 min four times.

Statistical analysis

The equality of variance in data was tested using Bartlett's test. For data with equal variance, the two-tailed Student's *t*-test or a one-way repeated measures analysis of variance (ANOVA) was used to determine significant differences between two or among multiple groups, respectively. If a significant result was determined using ANOVA ($P < 0.05$), the mean values of the control and the specific test group were analyzed using a Tukey-Kramer's test. Steel-Dwass's, Welch's test, Steel's test and Dunnett's test were used to determine significant differences between two specific groups or among multiple groups of interest. Randomization was used in each genotype, and data collection and analysis were not performed blind to the conditions of the experiments.

Supplementary Material

Supplementary Material is available at *HMG* online.

Acknowledgements

We thank Drs. JP. Vincent, V.I. Korolchuk, C.J. O'Kane, M. Guo, K. Matsuno, S. Hayashi, S.D. Renzis, and M. Farrer for providing materials, and we thank K. Yoshimi, Kakuta, T. Imura and C. Cui for their technical assistance.

Conflict of Interest statement. None declared.

Funding

Grants-in-Aid for Scientific Research (16K09679, 26860219 to T.I., 26293070 to Y.I., 15H04842 to N.H.) from JSPS in Japan and a Grant-in-Aid for Scientific Research on Innovative Areas (23111003 to N.H.) from MEXT in Japan and was partly supported by a grant from Otsuka Pharmaceutical (N.H. and Y.I.).

References

1. Vilarino-Guell, C., Wider, C., Ross, O.A., Dachsel, J.C., Kachergus, J.M., Lincoln, S.J., Soto-Ortolaza, A.I., Cobb, S.A., Wilhoite, G.J., Bacon, J.A. *et al*. (2011) VPS35 mutations in Parkinson disease. *Am. J. Hum. Genet.*, **89**, 162–167.
2. Zimprich, A., Benet-Pages, A., Struhal, W., Graf, E., Eck, S.H., Offman, M.N., Haubenberger, D., Spielberger, S., Schulte, E.C., Lichtner, P. *et al*. (2011) A mutation in VPS35, encoding a subunit of the retromer complex, causes late-onset Parkinson disease. *Am. J. Hum. Genet.*, **89**, 168–175.
3. Hierro, A., Rojas, A.L., Rojas, R., Murthy, N., Effantin, G., Kajava, A.V., Steven, A.C., Bonifacino, J.S. and Hurley, J.H. (2007) Functional architecture of the retromer cargo-recognition complex. *Nature*, **449**, 1063–1067.
4. Reddy, J.V. and Seaman, M.N. (2001) Vps26p, a component of retromer, directs the interactions of Vps35p in endosome-to-Golgi retrieval. *Mol. Biol. Cell*, **12**, 3242–3256.
5. Nothwehr, S.F., Bruinsma, P. and Strawn, L.A. (1999) Distinct domains within Vps35p mediate the retrieval of two different cargo proteins from the yeast prevacuolar/endosomal compartment. *Mol. Biol. Cell*, **10**, 875–890.
6. Gomez, T.S. and Billadeau, D.D. (2009) A FAM21-containing WASH complex regulates retromer-dependent sorting. *Dev. Cell*, **17**, 699–711.
7. Zavodszky, E., Seaman, M.N., Moreau, K., Jimenez-Sanchez, M., Breusegem, S.Y., Harbour, M.E. and Rubinsztein, D.C. (2014) Mutation in VPS35 associated with Parkinson's disease impairs WASH complex association and inhibits autophagy. *Nat. Ccommun.*, **5**, 3828.
8. McGough, I.J., Steinberg, F., Jia, D., Barbuti, P.A., McMillan, K.J., Heesom, K.J., Whone, A.L., Caldwell, M.A., Billadeau, D.D., Rosen, M.K. *et al*. (2014) Retromer binding to FAM21 and the WASH complex is perturbed by the Parkinson disease-linked VPS35(D620N) mutation. *Curr. Biol.*, **24**, 1670–1676.
9. Biskup, S., Moore, D.J., Celsi, F., Higashi, S., West, A.B., Andrabi, S.A., Kurkinen, K., Yu, S.W., Savitt, J.M., Waldvogel, H.J. *et al*. (2006) Localization of LRRK2 to membranous and vesicular structures in mammalian brain. *Ann. Neurol.*, **60**, 557–569.
10. Migheli, R., Del Giudice, M.G., Spissu, Y., Sanna, G., Xiong, Y., Dawson, T.M., Dawson, V.L., Galioto, M., Rocchitta, G., Biosa, A. *et al*. (2013) LRRK2 affects vesicle trafficking, neurotransmitter extracellular level and membrane receptor localization. *PLoS One*, **8**, e77198.
11. MacLeod, D.A., Rhinn, H., Kuwahara, T., Zolin, A., Di Paolo, G., McCabe, B.D., Marder, K.S., Honig, L.S., Clark, L.N., Small, S.A. *et al*. (2013) RAB7L1 interacts with LRRK2 to modify intraneuronal protein sorting and Parkinson's disease risk. *Neuron*, **77**, 425–439.
12. Cho, H.J., Yu, J., Xie, C., Rudrabhatla, P., Chen, X., Wu, J., Parisiadou, L., Liu, G., Sun, L., Ma, B. *et al*. (2014) Leucine-rich repeat kinase 2 regulates Sec16A at ER exit sites to allow ER-Golgi export. *EMBO J.*, **33**, 2314–2331.
13. Gomez-Suaga, P., Rivero-Rios, P., Fdez, E., Blanca Ramirez, M., Ferrer, I., Aiastui, A., Lopez De Munain, A. and Hilfiker, S. (2014) LRRK2 delays degradative receptor trafficking by impeding late endosomal budding through decreasing Rab7 activity. *Hum. Mol. Genet.*, **23**, 6779–6796.
14. Imai, Y., Gehrke, S., Wang, H.Q., Takahashi, R., Hasegawa, K., Oota, E. and Lu, B. (2008) Phosphorylation of 4E-BP by LRRK2 affects the maintenance of dopaminergic neurons in Drosophila. *EMBO J.*, **27**, 2432–2443.
15. Dodson, M.W., Leung, L.K., Lone, M., Lizzio, M.A. and Guo, M. (2014) Novel ethyl methanesulfonate (EMS)-induced null alleles of the Drosophila homolog of LRRK2 reveal a crucial role in endolysosomal functions and autophagy in vivo. *Dis. Model Mech.*, **7**, 1351–1363.
16. Imai, Y., Kobayashi, Y., Inoshita, T., Meng, H., Arano, T., Uemura, K., Asano, T., Yoshimi, K., Zhang, C.L., Matsumoto, G. *et al*. (2015) The Parkinson's Disease-Associated Protein Kinase LRRK2 Modulates Notch Signaling through the Endosomal Pathway. *PLoS Genet.*, **11**, e1005503.
17. Shin, N., Jeong, H., Kwon, J., Heo, H.Y., Kwon, J.J., Yun, H.J., Kim, C.H., Han, B.S., Tong, Y., Shen, J. *et al*. (2008) LRRK2 regulates synaptic vesicle endocytosis. *Exp. Cell Res.*, **314**, 2055–2065.
18. Lee, S., Liu, H.P., Lin, W.Y., Guo, H. and Lu, B. (2010) LRRK2 kinase regulates synaptic morphology through distinct substrates at the presynaptic and postsynaptic compartments of the Drosophila neuromuscular junction. *J. Neurosci.*, **30**, 16959–16969.

19. Piccoli, G., Condliffe, S.B., Bauer, M., Giesert, F., Boldt, K., De Astis, S., Meixner, A., Sarioglu, H., Vogt-Weisenhorn, D.M., Wurst, W. *et al.* (2011) LRRK2 controls synaptic vesicle storage and mobilization within the recycling pool. *J. Neurosci.*, **31**, 2225–2237.
20. Matta, S., Van Kolen, K., da Cunha, R., van den Bogaart, G., Mandemakers, W., Miskiewicz, K., De Bock, P.J., Morais, V.A., Vilain, S., Haddad, D. *et al.* (2012) LRRK2 controls an EndoA phosphorylation cycle in synaptic endocytosis. *Neuron*, **75**, 1008–1021.
21. Arranz, A.M., Delbroek, L., Van Kolen, K., Guimaraes, M.R., Mandemakers, W., Daneels, G., Matta, S., Calafate, S., Shaban, H., Baatsen, P. *et al.* (2015) LRRK2 functions in synaptic vesicle endocytosis through a kinase-dependent mechanism. *J. Cell Sci.*, **128**, 541–552.
22. Parisiadou, L., Yu, J., Sgobio, C., Xie, C., Liu, G., Sun, L., Gu, X.L., Lin, X., Crowley, N.A., Lovinger, D.M. *et al.* (2014) LRRK2 regulates synaptogenesis and dopamine receptor activation through modulation of PKA activity. *Nat. Neurosci.*, **17**, 367–376.
23. Linhart, R., Wong, S.A., Cao, J., Tran, M., Huynh, A., Ardrey, C., Park, J.M., Hsu, C., Taha, S., Peterson, R. *et al.* (2014) Vacuolar protein sorting 35 (Vps35) rescues locomotor deficits and shortened lifespan in Drosophila expressing a Parkinson's disease mutant of Leucine-Rich Repeat Kinase 2 (LRRK2). *Mol. Neurodegener.*, **9**, 23.
24. Beilina, A., Rudenko, I.N., Kaganovich, A., Civiero, L., Chau, H., Kalia, S.K., Kalia, L.V., Lobbestael, E., Chia, R., Ndukwe, K. *et al.* (2014) Unbiased screen for interactors of leucine-rich repeat kinase 2 supports a common pathway for sporadic and familial Parkinson disease. *Proc. Natl Acad. Sci. USA*, **111**, 2626–2631.
25. Franch-Marro, X., Wendler, F., Guidato, S., Griffith, J., Baena-Lopez, A., Itasaki, N., Maurice, M.M. and Vincent, J.P. (2008) Wingless secretion requires endosome-to-Golgi retrieval of Wntless/Evi/Sprinter by the retromer complex. *Nat. Cell Biol.*, **10**, 170–177.
26. Korolchuk, V.I., Schutz, M.M., Gomez-Llorente, C., Rocha, J., Lansu, N.R., Collins, S.M., Wairkar, Y.P., Robinson, I.M. and O'Kane, C.J. (2007) Drosophila Vps35 function is necessary for normal endocytic trafficking and actin cytoskeleton organisation. *J. Cell Sci.*, **120**, 4367–4376.
27. Shiba-Fukushima, K., Inoshita, T., Hattori, N. and Imai, Y. (2014) PINK1-mediated phosphorylation of Parkin boosts Parkin activity in Drosophila. *PLoS Genet.*, **10**, e1004391.
28. Wucherpfennig, T., Wilsch-Brauninger, M. and Gonzalez-Gaitan, M. (2003) Role of Drosophila Rab5 during endosomal trafficking at the synapse and evoked neurotransmitter release. *J. Cell Biol.*, **161**, 609–624.
29. Yun, H.J., Kim, H., Ga, I., Oh, H., Ho, D.H., Kim, J., Seo, H., Son, I. and Seol, W. (2015) An early endosome regulator, Rab5b, is an LRRK2 kinase substrate. *J. Biochem.*, **157**, 485–495.
30. Shimizu, H., Kawamura, S. and Ozaki, K. (2003) An essential role of Rab5 in uniformity of synaptic vesicle size. *J. Cell Sci.*, **116**, 3583–3590.
31. Verstreken, P., Kjaerulff, O., Lloyd, T.E., Atkinson, R., Zhou, Y., Meinertzhagen, I.A. and Bellen, H.J. (2002) Endophilin mutations block clathrin-mediated endocytosis but not neurotransmitter release. *Cell*, **109**, 101–112.
32. Ueno, T., Tomita, J., Tanimoto, H., Endo, K., Ito, K., Kume, S. and Kume, K. (2012) Identification of a dopamine pathway that regulates sleep and arousal in Drosophila. *Nat. Neurosci.*, **15**, 1516–1523.
33. Malik, B.R., Godena, V.K. and Whitworth, A.J. (2015) VPS35 pathogenic mutations confer no dominant toxicity but partial loss of function in Drosophila and genetically interact with parkin. *Hum. Mol. Genet.*, **24**, 6106–6117.
34. Zhao, X., Nothwehr, S., Lara-Lemus, R., Zhang, B.Y., Peter, H. and Arvan, P. (2007) Dominant-negative behavior of mammalian Vps35 in yeast requires a conserved PRLYL motif involved in retromer assembly. *Traffic*, **8**, 1829–1840.
35. Wang, H.S., Toh, J., Ho, P., Tio, M., Zhao, Y. and Tan, E.K. (2014) In vivo evidence of pathogenicity of VPS35 mutations in the Drosophila. *Mol. Brain.*, **7**, 73.
36. Munsie, L.N., Milnerwood, A.J., Seibler, P., Beccano-Kelly, D.A., Tatarnikov, I., Khinda, J., Volta, M., Kadgien, C., Cao, L.P., Tapia, L. *et al.* (2015) Retromer-dependent neurotransmitter receptor trafficking to synapses is altered by the Parkinson's disease VPS35 mutation p.D620N. *Hum. Mol. Genet.*, **24**, 1691–1703.
37. Ishizu, N., Yui, D., Hebisawa, A., Aizawa, H., Cui, W., Fujita, Y., Hashimoto, K., Ajioka, I., Mizusawa, H., Yokota, T. *et al.* (2016) Impaired striatal dopamine release in homozygous Vps35 D620N knock-in mice. *Hum. Mol. Genet.*, **25**, 4507–4517.
38. Tsika, E., Glauser, L., Moser, R., Fiser, A., Daniel, G., Sheerin, U.M., Lees, A., Troncoso, J.C., Lewis, P.A., Bandopadhyay, R. *et al.* (2014) Parkinson's disease-linked mutations in VPS35 induce dopaminergic neurodegeneration. *Hum. Mol. Genet.*, **23**, 4621–4638.
39. Pavlos, N.J. and Jahn, R. (2011) Distinct yet overlapping roles of Rab GTPases on synaptic vesicles. *Small GTPases*, **2**, 77–81.
40. Boucrot, E., Ferreira, A.P., Almeida-Souza, L., Debard, S., Vallis, Y., Howard, G., Bertot, L., Sauvonnet, N. and McMahon, H.T. (2015) Endophilin marks and controls a clathrin-independent endocytic pathway. *Nature*, **517**, 460–465.
41. Watanabe, S., Trimbuch, T., Camacho-Perez, M., Rost, B.R., Brokowski, B., Sohl-Kielczynski, B., Felies, A., Davis, M.W., Rosenmund, C. and Jorgensen, E.M. (2014) Clathrin regenerates synaptic vesicles from endosomes. *Nature*, **515**, 228–233.
42. Watanabe, S., Rost, B.R., Camacho-Perez, M., Davis, M.W., Sohl-Kielczynski, B., Rosenmund, C. and Jorgensen, E.M. (2013) Ultrafast endocytosis at mouse hippocampal synapses. *Nature*, **504**, 242–247.
43. Pavlos, N.J., Gronborg, M., Riedel, D., Chua, J.J., Boyken, J., Kloepper, T.H., Urlaub, H., Rizzoli, S.O. and Jahn, R. (2010) Quantitative analysis of synaptic vesicle Rabs uncovers distinct yet overlapping roles for Rab3a and Rab27b in Ca2+-triggered exocytosis. *J. Neurosci.*, **30**, 13441–13453.
44. Inoshita, T. and Imai, Y. (2015) Regulation of vesicular trafficking by Parkinson's disease-associated genes. *AIMS Mol. Sci.*, **2**, 461–475.
45. Deng, H.X., Shi, Y., Yang, Y., Ahmeti, K.B., Miller, N., Huang, C., Cheng, L., Zhai, H., Deng, S., Nuytemans, K. *et al.* (2016) Identification of TMEM230 mutations in familial Parkinson's disease. *Nat. Genet.*, **48**, 733–739.
46. Belenkaya, T.Y., Wu, Y., Tang, X., Zhou, B., Cheng, L., Sharma, Y.V., Yan, D., Selva, E.M. and Lin, X. (2008) The retromer complex influences Wnt secretion by recycling wntless from endosomes to the trans-Golgi network. *Dev. Cell*, **14**, 120–131.
47. Dodson, M.W., Zhang, T., Jiang, C., Chen, S. and Guo, M. (2012) Roles of the Drosophila LRRK2 homolog in Rab7-dependent lysosomal positioning. *Hum. Mol. Genet.*, **21**, 1350–1363.
48. Wu, T.H., Lu, Y.N., Chuang, C.L., Wu, C.L., Chiang, A.S., Krantz, D.E. and Chang, H.Y. (2013) Loss of vesicular

dopamine release precedes tauopathy in degenerative dopaminergic neurons in a Drosophila model expressing human tau. *Acta Neuropathol.*, **125**, 711–725.
49. Fabrowski, P., Necakov, A.S., Mumbauer, S., Loeser, E., Reversi, A., Streichan, S., Briggs, J.A. and De Renzis, S. (2013) Tubular endocytosis drives remodelling of the apical surface during epithelial morphogenesis in Drosophila. *Nat. Commun.*, **4**, 2244.
50. Entchev, E.V., Schwabedissen, A. and Gonzalez-Gaitan, M. (2000) Gradient formation of the TGF-beta homolog Dpp. *Cell*, **103**, 981–991.
51. Dong, B., Kakihara, K., Otani, T., Wada, H. and Hayashi, S. (2013) Rab9 and retromer regulate retrograde trafficking of luminal protein required for epithelial tube length control. *Nat. Commun.*, **4**, 1358.
52. Mori, Y., Koike, M., Moriishi, E., Kawabata, A., Tang, H., Oyaizu, H., Uchiyama, Y. and Yamanishi, K. (2008) Human herpesvirus-6 induces MVB formation, and virus egress occurs by an exosomal release pathway. *Traffic*, **9**, 1728–1742.
53. Imai, Y., Soda, M. and Takahashi, R. (2000) Parkin suppresses unfolded protein stress-induced cell death through its E3 ubiquitin-protein ligase activity. *J. Biol. Chem.*, **275**, 35661–35664.